Article:
Sherman, DM and Peacock, CL (2010) Surface complexation of Cu on birnessite (d-MnO2): Controls on Cu in the deep ocean. Geochimica et Cosmochimica Acta, 74 (23). pp. 6721-6730. ISSN: 0016-7037

https://doi.org/10.1016/j.gca.2010.08.042

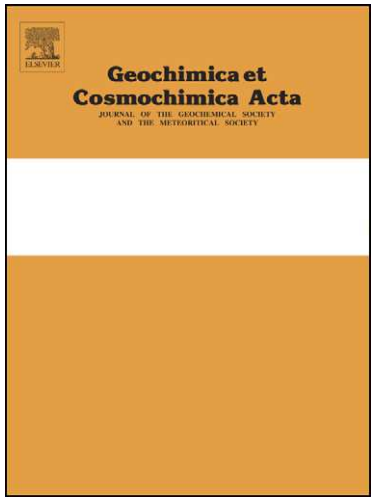

Surface Complexation of Cu on Birnessite (δ-MnO_2): Controls on Cu in the Deep Ocean

David M. Sherman, Caroline L. Peacock

PII: S0016-7037(10)00505-3
DOI: 10.1016/j.gca.2010.08.042
Reference: GCA 6914

To appear in: *Geochimica et Cosmochimica Acta*

Received Date: 26 October 2009
Accepted Date: 26 August 2010

Please cite this article as: Sherman, D.M., Peacock, C.L., Surface Complexation of Cu on Birnessite (δ-MnO_2): Controls on Cu in the Deep Ocean, *Geochimica et Cosmochimica Acta* (2010), doi: 10.1016/j.gca.2010.08.042

Surface Complexation of Cu on Birnessite (δ-MnO_2): Controls on Cu in the Deep Ocean

David M. Sherman*[1] and Caroline L. Peacock[2]

[1] Department of Earth Sciences
University of Bristol
Bristol BS8 1RJ, UNITED KINGDOM

[2]School of Earth and Environment
University of Leeds
Leeds, LS2 9JT, UNITED KINGDOM

Revised 22 July 2010

Submitted to Geochimica et Cosmochimica Acta

*Corresponding author: e-mail: *dave.sherman@bris.ac.uk*

Index Terms: *copper, birnessite, marine ferromanganese crusts, manganese nodules, seawater, EXAFS, surface complexation, density functional calculations*

Running Head: *Surface complexation of Cu on birnessite (δ-MnO_2)*

ABSTRACT

Hexagonal birnessite (-MnO_2) is a close analogue to the dominant phase in hydrogenetic marine ferromanganese crusts and nodules. These deposits contain ~0.25 wt. % Cu which is believed to be scavenged from the overlying water column where Cu concentrations are near 0.1 µg/L. Here, we measured the sorption of Cu on -MnO_2 as a function of pH and surface loading. We characterized the nature of the Cu sorption complex at pH 4 and 8 using EXAFS spectroscopy and find that, at pH 4, Cu sorbs to birnessite by inner-sphere complexation over the vacancy site to give a 3- to 4-fold coordinated complex with 6 Mn neighbors at ~3.4 Å. At pH 8, however, we find that some Cu has become structurally incorporated into the MnO_2 layer by occupying the vacancy sites to give 6 Mn neighbors at ~2.91 Å. Density functional calculations on $CuMn_{18}O_{24}(OH)_{30}(H_2O)_3^{-4}$ and $CuMn_{18}O_{21}(OH)_{33}(H_2O)_3^{-1}$ clusters predict a 3-fold coordinated surface complex and show that the change from surface complexation to structural incorporation is a response to protonation of oxygens surrounding the vacancy site. Consequently, we propose that the transformation between sorption via surface complex and vacancy site occupancy should be reversible. By fitting the Cu sorption as a function of surface loading and pH to the formation of the observed and predicted surface complex, we developed a surface complexation model (in the basic Stern approximation) for the sorption of Cu onto birnessite. Using this model, we demonstrate that the concentration of inorganic Cu in the deep ocean should be several orders of magnitude lower than the observed total dissolved Cu. We propose that the observed total dissolved Cu concentration in the oceans reflects solubilization of Cu by microbially generated ligands.

1. INTRODUCTION

The depth-concentration profile of Cu in the oceans is intermediate between that characteristic of scavenged and nutrient elements (Bruland & Lohan, 2004). Dissolved copper is strongly scavenged by sorption to colloidal iron and manganese oxides; these accumulate to form ferromanganese crusts and nodules with Cu concentrations enriched by 10^6 over average seawater concentration (Arrhenius, 1963). In addition to being scavenged, dissolved Cu^{+2} is complexed by microbially generated ligands which may play a role in detoxifying Cu (Coale and Bruland, 1988; Bruland and Lohan, 2004). There is recent evidence that such ligands may be significant for Cu even in the deep ocean (Moffat and Dupont, 2007).

Within ferromanganese crusts, Cu tends to be more strongly associated with the manganese oxide phase (Cronan, 1969; Kumar et al., 1994). The nature of the manganese oxide phases and the mechanism by which such minerals become highly enriched in trace metals is still unclear. The dominant manganese oxide phase in marine ferromanganese precipitates is birnessite (Burns and Burns, 1979). Birnessite is a phyllomanganate consisting of sheets of edge-sharing MnO_6 octahedra; the sheets yield X-ray diffraction lines at 2.4 Å and 1.4 Å. In well-crystalline birnessites, the sheets of edge-sharing MnO_6 octahedra are stacked in the c-direction to give additional diffraction lines at ~7 Å (001) and ~3.6 Å (002). However, marine birnessites usually show only diffraction lines at 2.4 and 1.4 Å and are termed "vernadite" or δ-MnO_2. The absence of the ~7 Å (001) and ~3.6 Å (002) lines is due to a lack of coherent stacking order of the MnO_6 sheets in the c-direction.

In addition to the degree of stacking order, natural and synthetic birnessites show variations in the oxidation state and fraction of vacancies within the MnO_6 sheet. Natural marine birnessites have all Mn as Mn(IV) (Murray et al., 1984) and hexagonal symmetry (Jones and Milne, 1956; McKenzie, 1989; Post, 1992). Drits et al. (1997) showed that this symmetry results from ordered vacancies in the octahedral sites. Sorption of Ni on synthetic hexagonal-birnessites occurs via complexation over vacancy sites (Peacock and Sherman, 2007a; Manceau et al., 2007), as does sorption of Cu (Manceau et al., 2002). With increasing pH, however, surface-complexed Ni cations move into the vacancy site and become structurally incorporated (Peacock and Sherman, 2007a; Peacock and Sherman, 2007b). Significantly, this transition between surface complexation and structural incorporation has been demonstrated to be reversible (Peacock, 2009). For -MnO_2, Villalobos et al. (2006)

report 0.06 vacancies per Mn octahedron although a more recent study indicates the number of vacancies per octahedron may be higher (Grangeon et al., 2008). This suggests that hexagonal birnessites may sorb transition metals in excess of 6 mole % via complexation over vacancy sites.

The sorption of Cu to birnessite is rapid (compared to its oceanic residence time) and we hypothesize that dissolved Cu in the oceans is in chemical equilibrium with birnessite. To develop this hypothesis further, we need a thermodynamic model for the uptake (scavenging) of Cu by phases such as -MnO_2. This model would enable us to predict how dissolved Cu concentrations might respond to anthropogenic perturbations and may help us decipher how paleochemical records indicate past chemical perturbations (e.g., changes in pH and inputs due to hydrothermal fluxes). In the work presented here, we report results of sorption experiments of copper to synthetic birnessite as a function of pH and concentration. We characterize the nature of the sorption complexes using EXAFS spectroscopy and *ab initio* (density functional) predictions of the structures and energetics of model clusters that correspond to possible sorption complexes. We then fit the sorption edges to a surface complexation model based on the sorption complexes determined from EXAFS and ab initio simulations. From this model, we attempt to predict the equilibrium distribution of Cu between seawater and ferromanganese crusts.

2. EXPERIMENTAL AND COMPUTATIONAL METHODS

2.1. Mineral preparation and characterisation

As shown by Murray et al. (1984), the Mn oxides which occur in marine ferromanganese nodules and crusts have Mn entirely as Mn(IV). Synthetic birnessites can have variable oxidation states of Mn with charge compensation provided by H^+ or Na, K cations. The ™-MnO_2 form of birnessite was prepared by following the synthesis procedure outlined in Villalobos et al. (2003) based on the reaction:

$$2KMnO_4 + 3MnCl_2 + 4NaOH \rightarrow 5MnO_2 + 2KCl + 4NaCl + 6H_2O \quad (1)$$

to yield a product which Villalobos et al. (2003) demonstrated had all of the Mn as Mn(IV). The Mn K-edge XANES of the ™-MnO_2 used here is identical to that of the -MnO_2 phase in Villalobos et al. (2003). Iodometric titration of our product was unable to detect Mn^{+3}, this is

consistent with the synthesis product of Villalobos et al. (2003). However, Grangeon et al. (2008) have reanalyzed the Villalobos et al. (2003) birnessite using a Mohrs salt titration method and found an average oxidation state of 3.9. The significance of any trace Mn^{+3} to the sorption of metals to birnessite is unclear. X-ray diffraction patterns of the dried product show asymmetric peaks at ~7 Å, 2.4 Å and 1.4 Å in agreement with the product described in Villalobos et al. (2003). The surface area (measured using the BET method), is 107 m^2/g. As will be shown below, however, this surface area greatly underestimates the sorption capacity of the birnessite.

We measured the experimental pH_{PZC} of our -MnO_2 by potentiometric titration at two salt concentrations (0.01 and 0.1 M $NaNO_3$). Freshly prepared, air-dried -MnO_2 (0.83 g/L) was suspended in pre-boiled, nitrogen purged (<1 ppm CO_2 (g)) 18.2 mΩ MilliQ water, and nitrogen purged (<1 ppm CO_2 (g)) for several hours. Titrations were performed at 25 °C in an air-tight vessel with constant stirring to avoid settling. Base (NaOH, free from carbonate), acid (HNO_3) and salt solutions ($NaNO_3$) were added via an automated titrator. A nitrogen atmosphere (<1 ppm CO_2 (g)) was maintained throughout the experiment. Electrolyte was added to bring the ionic strength to 0.01 M and then acid added gradually to lower the pH to ~1.5. Incremental addition of base then produced a titration from acid pH to pH ~9. After each incremental addition of base, up to 5 mins were allowed for pH equilibration. The suspension was returned to acid pH by reverse acid titration, electrolyte added to adjust the ionic strength to the next level and the titration repeated following the same method. No significant hysteresis was observed between the base and acid legs. We find pH_{PZC} = 2.3 ± 0.2 and this is in good agreement with previous acid-base titrations of -MnO_2 (e.g., Catts and Langmuir, 1986).

2.2. Cu vs. pH adsorption edge experiments

Batch sorption edge experiments were prepared with Cu(II) aqueous solution using AR grade reagents and 18.2 m Milli-Q water. All solutions and resulting suspensions were purged with N_2 (g) (<1 ppm CO_2 (g)) and all adsorption experiments were conducted at 25 °C. pH measurements were calibrated to ±0.05 pH units using Whatman NBS grade buffers.

Copper(II) stock solution was prepared at 1000 ppm from $Cu(NO_3)_2.3H_2O$ in 0.1 M HNO_3. $NaNO_3$ stock solution was prepared at 0.1 M for use as background electrolyte. Adsorption experiments at 143, 77 and 32 ppm $[Cu]_{total}$ were prepared by adding 5, 2.5, and 1

ml of 1000 ppm Cu stock solution to 0.100 g solid δ-MnO_2 to 30 mL of 0.1 M $NaNO_3$, respectively. Adsorbent concentration was therefore 3.3 g/L, with the adsorbent containing ~ 5, 2.5 and 1 wt.% Cu at 100% adsorption, respectively. Stock solution was added incrementally after ~pH 5.5 to avoid the possible precipitation of solid Cu (hydr)oxide phases (Cu speciation in our experimental solutions was calculated using PHREEQC (Parkhurst and Appelo, 1999) and the MINTEQ.V4 database (Charlton and Parkhurst, 2002)). The resulting suspensions were immediately shaken. Suspension pH was varied between pH 1-7 by the dropwise addition (<1 mL) of either HNO_3 or NaOH and recorded after stabilization to two decimal places. Adsorption edge experiments were then shaken continuously for 1 week during which pH values were adjusted using NaOH or HNO_3. Final pH measurements were obtained for the experimental suspensions before centrifugation or filtering.

All adsorption suspensions were separated by centrifugation (~3000 g for 10 min) into an adsorption sample (thick paste) and a clear supernate for determination of total Cu concentration. Thick paste adsorption samples at pH 4 and 8 and with 5 wt.% Cu were subject to EXAFS after storing at 1 – 4 $^{\circ}$C for a maximum of 48 hours before scanning. Supernates were filtered using 0.2 µm cellulose nitrate membrane filters, acidified with 1% HNO_3 and analyzed for Cu by inductively-coupled plasma atomic emission spectroscopy (ICP-AES). Supernates from the experiments used for EXAFS (at pH 4 and 8 and with 5 wt.% Cu) were analysed for Cu and Mn by ICP-MS. Cu and Mn analytical detection limits were better than 10 ppb. Aqueous Mn was <100 ppb for both EXAFS sample supernates.

2.3. EXAFS spectra of Cu sorption complexes

EXAFS data were collected at the CCLRC Synchrotron Radiation Source at Daresbury Laboratory, U.K. Spectra of the Cu K-edge (8979 eV) were collected on station 16.5, which was designed for measurements on ultra-dilute systems. During data collection, storage ring energy was 2.0 GeV and the beam current varied between 130 and 240 mA. Adsorption samples were presented to the X-ray beam as a wet paste held in a 2 mm-thick Teflon slide with a 4 x 10 mm sample slot. Small sheets of 250 µm-thick Mylar were placed on either side of the Teflon slide and sealed with a small amount of vacuum grease to hold the wet pastes in place and prevent drying of the samples. EXAFS data were collected from up to 20 fluorescence mode scans using an Ortec 30-element solid-state detector.

EXAFS data reduction was performed using Daresbury Laboratory software (EXCALIB and EXBACK, Dent and Mosselmans, 1992). EXCALIB was used to calibrate

from monochromator position (millidegrees) to energy (eV) and to average multiple spectra from individual samples. EXBACK was used to define the start of the EXAFS oscillations (determined from the inflection point on the K-edge) and perform background subtraction. The pre-edge was fit to a linear function and the post-edge background to two 2^{nd}-order polynomial segments. The phase-shifts and potentials were calculated in the small atom (plane-wave) approximation and we allowed for multiple scattering as coded in EXCURV98 (Binsted, 1998). The phase-shift functions used in the curve fitting were derived by *ab initio* methods in EXCURV98 using Hedin-Lundqvist potentials (Hedin and Lundqvist, 1969) and von Barth ground states. No Fourier filtering was performed during the data analysis. Typical errors associated with EXAFS modelling over the k-range used here are 15 % and 25 % for first and second shell coordination numbers, respectively, ± 0.02 and 0.05 Å for first and second shell distances, respectively, and 15 % and 25 % for first and second shell Debye-Waller factors, respectively (Binsted, 1998).

2.4. Density functional theory calculations

Quantum mechanical calculations on $CuMn_{18}O_{24}(OH)_{30}(H_2O)^{-4}$ and $CuMn_{18}O_{21}(OH)_{33}(H_2O)^{-1}$ clusters were used to predict bond lengths and energies of proposed Cu sorption complexes. Calculations were done using the ADF code of te Velde et al. (2001). ADF implements density functional theory for finite clusters and molecules using the linear combination of atomic orbital formalism. For all atoms except hydrogen, we used frozen core orbitals (i.e., 1s, 2s, 2p, 3s and 3p for Mn and Cu; 1s for O). Molecular orbitals in the ADF code are constructed from Slater type atomic orbitals which consist of a cartesian part $r^{kr}x^{kx}y^{ky}z^{kz}$ with $k_x+k_y+k_z = l$ (l = angular momentum quantum number) and an exponential part $e^{-(r}$. For all atoms, we used an uncontracted, triple-zeta basis set with polarization functions (Van Lenthe and Baerends, 2003). No optimization of the basis set was done. With this basis set, counterpoise corrections for basis set superposition energy, evaluated by replacing a Cu with a ghost atom in a simple $Cu(H_2O)_6^{+2}$ cluster, are found to be negligible (< 1 kJ/mole).

The calculations were done using the PBE version (Perdew et al., 1996) of the generalized gradient approximation (GGA) of the exchange-correlation functional (Perdew et al., 1992). All calculations were done using the spin-unrestricted formalism to account for the

three unpaired 3d-electrons of Mn and the 1 unpaired 3d-electron of Cu; in each cluster, the Mn and Cu atoms were set up in a ferromagnetic configuration. The geometries of the clusters were optimized using a Newton-Raphson method and Broydon-Fletcher update of the Hessian matrix as coded in ADF. The total energies of each complex during geometry optimizations were converged to ± 0.3 kJ/mole.

2.5. Surface complexation modelling

Surface complexation modelling was done using a FORTRAN90 program EQLFOR (Sherman et al., 2008; Sherman, 2009) based on the original "tableau" speciation algorithm described by Morel and Morgan (1972). Modifications to the mass balance, Jacobian and convergence routines were made to include the surface and diffuse layer charges of the basic (2 layer) Stern model (Sherman, 2009). Equilibrium constants for surface complexes were derived by fitting all sorption edges simultaneously. The speciation routines are called by a gradient search fitting algorithm (Bevington and Robinson, 2002) to optimize the equilibrium constants. The fitting was obtained by minimizing χ^2, which is calculated assuming a relative error of 2 % in concentrations/pH.

In the Morel and Morgan (1972) method, the speciation is calculated using mass balance constraints to give the molal concentrations of surface species. The correct thermodynamic formulation (i.e., one that gives the correct ideal configurational entropy of a species) of the activity of a surface species is in terms of the mole fraction of surface sites occupied by the species. The resulting stability constants are obtained from the apparent (fitting to mass balance) stability constants by converting the concentration of each surface species to its mole fraction. Activity corrections to the stability constants for aqueous species were made using the Davies equation.

3. RESULTS AND DISCUSSION

3.1. Sorption of Cu on birnessite

The sorption of Cu to birnessite at several different surface loadings is shown in Figure 1. The results obtained here are very different from those obtained by Catts and Langmuir (1986) and Fu et al. (1991). In those experiments, the Cu sorption edge occurs at ~2 pH units higher for similar degrees of loading (Figure 1). Both of those studies used a birnessite or δ-MnO_2 phase synthesized by reacting solutions of Mn^{+2} and $KMnO_4$. X-ray

diffraction of the phases used by these authors are reported to have the same diffraction lines as those obtained here; however, the intensities of the (001) and (002) reflections are unknown. A highly crystalline birnessite in which the phyllomanganate sheets are stacked in the c-direction will have a smaller fraction of vacancy sites relative to edge-sites available for surface complexation. The discrepancies between the results obtained here and those reported by previous authors may reflect differences in the crystallinity of the birnessite. Marine birnessites typically show no (001) reflection and, consequently, surface complexation should be dominated by vacancy rather than edge-site sorption.

3.2 EXAFS of Cu sorbed to birnessite

EXAFS spectra of Cu sorbed to birnessite (5.0 wt. %) at pH 4 and 8 are shown in Figure 2. The Fourier transform of the EXAFS of Cu-birnessite at pH 4 indicates a first coordination shell containing ~4 oxygen atoms near 1.95 Å and a further coordination shell corresponding to ~6 Mn near 3.4 Å. We interpret this as indicating a Cu surface complex formed over a vacancy site; consequently, we forward-modelled the EXAFS spectrum using the cluster shown in Figure 3a. During the fit, we refined a total of 9 parameters (the correction to the Fermi energy (EF), 2 Cu-O distances, 2 Cu-Mn distances and 4 Debye-Waller factors (DWF's). These are given in Table 1. Stern's rule (Stern, 1993) limits the number of independent data parameters N_{ind} as $2\Delta k\Delta R/\pi + 2$ (Booth and Hu, 2009) where Δk and ΔR are the range in k- and R-space actually fitted. For our experiment, $N_{ind} = 15$; hence our model should not be over-fitting the data. Note that the apparent resolution of the two Mn shells at 3.39 and 3.43 Å is not statistically significant since such small differences in Cu-Mn distances cannot be resolved with the k-range used. The two distances simply reflect the symmetry of the cluster used.

Our model for Cu-birnessite at pH 4 differs somewhat from the interpretation of Manceau et al. (2002); they fit their EXAFS of Cu-birnessite at pH 4 (described in Lanson et al., 2002) to 4 O at 1.96 Å and two O at 2.23 Å, with a much larger DWF, as expected for Cu in a Jahn-Teller distorted environment. However, we cannot resolve the second oxygen shell in our fit. Moreover, we do not expect Cu to be in 6-fold coordination when complexed to a surface vacancy. First, our predicted geometries from density functional calculations on a Cu surface complex cluster (discussed below) do not predict 6-fold coordination of Cu. Secondly, it is now realized that the coordination number of Cu^{+2} in aqueous solution is actually 5 (Pasquarello et al., 2001; Amira et al., 2005). On the other hand, we are in good

agreement with the interpretation of Manceau et al. (2002) regarding the outer shell of 6 Mn atoms near 3.43 Å and we also find no evidence for Cu sorption at edge sites or for Cu surface precipitation.

The EXAFS of Cu sorbed at pH 8 is similar to that at pH 4 except that there is an additional scattering due to Mn atoms near 2.9 Å. This indicates a second coordination environment of Cu; we interpret this as Cu occupying a vacancy site. To forward-model the EXAFS of Cu sorbed at pH 8, we used two clusters simultaneously: a surface complex cluster (Figure 3a) and a cluster corresponding to Cu occupying the vacancy site (Figure 3b). From the fit, we estimate that ~20 % of the Cu has occupied the vacancy site. The calculated fit parameters are given in Table 1. The Cu EXAFS at pH 8 was refined with total of 12 parameters (EF, 2 Cu-O distances, 3 Cu-Mn distances, 5 DWF's and the fraction of Cu occupying a vacancy (see Table 1)). Since this is less than N_{ind} for the k- and r-ranges used, we have not over-fit the data. However, as with the surface complex cluster, the apparent resolution between the two Mn shells at 2.81-2.91 Å in cluster 2 is not statistically significant since such small differences in Cu-Mn distances cannot be resolved with the k-range used.

By analogy with Ni (Peacock and Sherman, 2007a), a surface complex formed on the edge-sites of birnessite (as opposed to a complex formed over a vacancy), would have a Cu-Mn distance intermediate between that found for the vacancy complex and solid solution. Including such an edge complex is not necessary to fit the EXAFS; consequently, although edge-complexes may be present they cannot be resolved.

3.3 DFT Optimized geometries and energetics of surface complexes

The optimized structures and energies of clusters corresponding to Cu sorbed as a surface complex and Cu occupying a vacancy sites are shown in Figures 4 and 5. The geometry of the surface complex predicts the Cu will be in 3-fold coordination in an approximately trigonal arrangement with an average Cu-O bond length of 1.93 Å and an average Cu-Mn distance of 3.29 Å. Note that the water molecules in Figure 5 are > 3Å away from the Cu atom and not part of its coordination shell. The predicted average Cu-O distance is in good agreement with that observed (1.95 Å) using EXAFS, although the EXAFS were fit to four nearest neighbor oxygens. However, in the EXAFS fit, the DWF of the fourth oxygen is quite large (0.02). The difference in coordination number between that predicted and that derived from the EXAFS may simply reflect the uncertainty in the DWF's and coordination numbers derived from EXAFS. The predicted average Cu-Mn distance (3.29 Å) is 4 %

smaller than that observed using EXAFS. The origin of this discrepancy is unclear but might, for example, reflect longer range structural relaxation associated with next nearest-neighbor vacancies. The discrepancy might also reflect a dependence of the Cu-Mn distance on the protonation state of the vacancy oxygen as discussed below.

If Cu occupies the vacancy site (solid solution) instead of forming a surface complex, the expected Jahn-Teller distortion gives Cu-O distances of 2.0 (x2), 2.1 (x 2) and 2.2 (x2) to give an average distance of 2.1 Å which is about 8 % higher than those observed with EXAFS; however, the experimental Cu-O distance is poorly constrained due to overlap with the Cu-O scattering in the surface complex. The predicted average Cu-Mn distance of 2.92 Å is in good agreement with the EXAFS result of ~2.9 Å where this peak is well resolved.

The cluster calculations, moreover, provide insight on sorption via surface complexation vs. sorption via solid solution. When the oxygen atoms surrounding the vacancy site are not protonated, the surface complex cluster is calculated to be 40 kJ/mole less stable than the cluster with Cu occupying the vacancy site. However, if the opposite three oxygens surrounding the vacancy site are protonated as in Figure 4, the surface complex is 40 kJ/mole more stable than the complex having Cu occupy the vacancy site. This could explain why Cu forms only a surface complex at low pH but occupies a vacancy site at high pH. A more quantitative understanding of the relative proton affinities of the surface oxygen sites on birnessite is needed before we can predict the protonation of the surface oxygens as a function of pH. Unfortunately, we still have an incomplete understanding of the surface protonation of goethite (⟨-FeOOH) even though the goethite surface has received far more attention than that of birnessite (e.g., Sherman, 2009 and references therein).

3.4. Surface complexation modelling

The batch sorption experiments show that the Cu sorption edge occurs below pH 4. EXAFS results indicate that sorbed Cu forms a surface complex at this pH but starts to occupy vacancy sites at high pH. The optimized structures and energies of clusters corresponding to Cu sorption complexes suggest that the transformation between surface complex and incorporation into the vacancy sites is a response to changes in the protonation state of the vacancy site oxygens. Given this molecular understanding of Cu sorption, we can now fit the sorption edges to a surface-complexation model. To this end, we need to know the surface site densities and the protonation of the birnessite surface oxygens.

3.4.1 Surface site densities

As discussed above, at the loading used here, Cu sorbs to birnessite by forming an inner-sphere complex above (and in) the vacancy sites. An idealized birnessite consisting of randomly stacked $H_4Mn_5O_{24}$ layers with a vacancy structure, as described in the model for the 1H phase of hexagonal birnessite (Lanson et al., 2000), would have 2.22 vacancy sites per nm^2. However, the structural model of Villalobos et al. (2006) for δ-MnO_2 has only 0.8 vacancies per nm^2. Assuming a maximum reactive surface area of 611 m^2/g (i.e., only half of the surface area of a single phyllomanganate sheet is counted assuming only 1 Cu atom can complex on each vacancy), we find the maximum sorption capacity for Cu would be 5.15 wt. %. However, given the measured BET surface area of 107 m^2/g for the birnessite used here, the sorption capacity should be only 0.9 wt% Cu. This is well below that observed in the batch absorption experiments; the EXAFS at 5 wt. % loading do not show evidence for any $Cu(OH)_2$ phase or resolvable evidence for complexes on particle edges. Consequently, we conclude that the BET surface greatly underestimates the reactive surface area of birnessite. This has been shown to be the case for ferrihydrite (Dzombak and Morel, 1990). Because of our uncertainty in the reactive surface area and in the number of available vacancy sites on the {001} surfaces, the surface complexation modelling discussed below was done by using the number of reactive sites as an adjustable parameter. Since sorption edges at three different loadings were measured, it was possible to optimize the fit to the number of reactive sites.

3.4.2 Surface protonation

We modeled the protonation of {001} surface oxygens on δ-MnO_2 using the equilibrium

$$>Mn_2O^{-2/3} + H^+ = >Mn_2OH^{+1/3} \qquad (2a)$$

$$K_a = \frac{\{>Mn_2OH^{+1/3}\}}{\{>Mn_2O^{-2/3}\}[H^+]} \exp\left(-\frac{\Psi_0 F}{RT}\right) \qquad (2b)$$

where Ψ_0 is the electrostatic potential at the 0-plane, R is the gas constant, F is the Faraday constant and T is temperature. We use the log $K_a = 2.3$ for reaction (2a) from the potentiometric titration done described above. Here, and in what follows, we define the (ideal) activity of a surface complex as the mole fraction of the surface sites that it occupies (this is relative to a standard state of complete coverage). This

372 definition gives the correct treatment of the configurational entropy and for multidentate
373 complexes this approach is essential (e.g., Tadanier and Eick, 2002). The surface
374 electrostatic potential ψ_0 is defined from the surface charge distribution using the basic Stern
375 model (Westall and Hohl, 1980). In the basic Stern model, the Stern layer (i.e., that between
376 the 0-plane and 1-plane) has a capacitance of $C_{stern} = \varepsilon_0\varepsilon_s/d$ where ε_0 is the permittivity of a
377 vacuum (8.854×10^{-12}), ε_s is the Stern layer dielectric constant and d is the distance of charge
378 separation in meters (assumed to be the average distance of approach of hydrated counter
379 ions). Assuming d is ~ 4 Å and that the dielectric constant is intermediate between that of
380 pure water (78) and water at dielectric saturation (6), we estimate a Stern layer capacitance of
381 1 F/m^2. This is comparable to that used by Boily et al. (2001) for goethite. However,
382 changing the capacitance by ± 0.5 F/m^2 had a negligible effect on the goodness of fit or the
383 equilibrium constants for the sorption edges measured here.
384 For the surface protonation reactions, the change in charge is assigned to the 0-plane.
385 Following the approach used by previous workers (e.g., Hiemstra and Van Riemsdijk, 1996)
386 for iron oxides, we assign a formal reference charge -2/3 to oxygens in the Mn_2O surface
387 groups based on Pauling's second rule. (Note that it is only the change in surface charge that
388 contributes to the free energy of sorption; the assignment of a formal charge to surface sites is
389 simply to enable charge conservation in the mass-balance equations used when fitting the
390 sorption data to a surface complexation model).
391
392 *3.4.3 Cu surface complexation model*
393 Based on the results from EXAFS spectroscopy, we will neglect any complexes
394 forming at the particle edges and assume that Cu^{+2} only forms complexes with the three
395 $>Mn_2O^{-2/3}$ oxygens associated with vacancy sites on the {001} surface. We assume that the
396 $>Mn_3O^0$ surface sites on {001} do not protonate or form complexes with Cu^{+2}. The
397 formation of the surface complex is then:
398
399 $$3(>Mn_2O^{-2/3}) + Cu^{+2} = (>Mn_2O)_3Cu^0 \qquad (3a)$$
400
401 with conditional (I = 0.1 M) equilibrium constant:
402

$$K_s = \frac{\{(> Mn_2O)_3 Cu^0\}}{\{> Mn_2O^{-2/3}\}^3 [Cu^{+2}]} \exp\left(-\frac{2\Psi_0 F}{RT}\right) \quad (3b)$$

where $\{(>Mn_2O)_3Cu^0\}$ is the mole fraction of {001} surface $>Mn_2O$ sites occupied by the $(>Mn_2O)_3Cu^0$ complex. We assign all of the change in surface charge due Cu^{+2} adsorption (+2) to the change in charge of the 0-plane. The optimized value of log K_S = 5.63. The one-site surface complexation model fits to the Cu-birnessite adsorption data are shown on Figure 1. The sorption edges (pH < 5) are fit to only the $(>Mn_2O)_3Cu^0$ surface complex. The transformation of the surface complex to the occupied vacancy site at high pH is not included in the sorption equilibria. This means that we are not completely describing the surface electrostatic contribution to the surface sorption at high pH. If Cu atoms occupying the vacancy sites can disorder to form a complete solid solution with Mn, then we are not correctly including the entropy of mixing. Neglect of these effects suggests that our model will underestimate the sorption of Cu to birnessite at high pH (e.g., as in seawater).

3.5 Application to the Deep Ocean

Using our surface complexation model, we can estimate an upper limit for the dissolved concentration of inorganic Cu^{+2} (e.g., Cu^{+2}, $CuOH^+$ and $CuCO_3$) that would be in chemical equilibrium with a ferromanganese crust with 0.25 wt. % Cu. For a marine birnessite with 1.1 x 10^{-3} moles of vacancy sites/g, as estimated for the birnessite used in this study (Table 2), this corresponds to a mole fraction of ~0.035 surface sites complexed to Cu. To estimate the concentration of dissolved Cu in seawater, we implemented our surface complexation model in PHREEQC (Parkhurst and Appello, 1999) together with the MINTEQ.V4 database (Charlton and Parkhurst, 2002) and a solution with the major ion composition of seawater. We find that, at pH 7-8, a birnessite with 0.25 wt. % Cu would be in equilibrium with a dissolved inorganic Cu^{+2} concentration < 10^{-6} nmolkg^{-1}. This is many orders of magnitude below that observed (~4 nmolkg^{-1}); we conclude that essentially all dissolved Cu in deep ocean seawater must be present in chelated form. This is consistent with the observed deep-water complexation of Cu observed by Moffet and Dupont (2007).

Acknowledgements - We are grateful to Ewa Bednarz for help with the sorption experiments and to Chung Choi (University of Bristol) for ICP-AES measurements. We are especially grateful to Bob Bilsborrow, station manager of 16.5 at the Daresbury Synchrotron radiation source, for his help in optimising the experimental conditions. We are also grateful for the helpful comments of four anonymous reviewers and the Associate Editor. Synchrotron beamtime was provided by direct access awards from CCLRC. This work was supported by NERC Grant NER/B/S/2003/00293.

441 REFERENCES

442 Amira S., Spangberg D., Hermansson K. (2005) Distorted five-fold coordination of Cu2+
443 (aq) from a Car-Parrinello molecular dynamics simulation, *Phys. Chem. Chem. Phys.*,
444 **7**, 2874-2880.
445 Arrhenius G. (1963) Pelagic sediments. In: M. N. Hill (ed.) The sea: ideas and observations
446 on progress in the study of the seas, vol. 33, 655-718. Interscience, New York.
447 Bevington, P. and Robinson, D.K. (2002) Data Reduction and Error Analysis for the physical
448 sciences. McGraw-Hill, New York 326 pp.
449 Binsted, N. (1998) *SERC Daresbury Laboratory EXCURV98 program.* Daresbury
450 Laboratory, Warrington, U.K.
451 Boily J-F., Lützenkirchen J., Balmés O., Beattle J., and Sjöberg S. (2001) Modelling proton
452 binding at the goethite (a-FeOOH)-water interface. Colloids and Surfaces A:
453 Physicochemical and Engineering Aspects, **179**, 11-27.
454 Booth C. H., Hu Y-J. (2009) Confirmation of standard error analysis techniques applied to
455 EXAFS using simulations. *Journal of Physics: Conference series* **190**, 1-6.
456 Bruland K.W., and Lohan M.C. (2004) The control of trace metals in seawater. Chpt 2 in
457 *The Oceans and Marine Geochemistry*, Vol. 6 (Ed. Harry Elderfield) in Treatise on
458 Geochemistry (Eds. H.D. Holland and K.K. Turekian), 6, 34-47.
459 Burns R.G., and V.M. Burns (1979) Manganese oxides, in Marine Minerals (R.G. Burns,
460 Ed.). Reviews in Mineralogy, 6, 1-46. Mineralogical Society of America, Washington,
461 D.C.
462 Catts J. G., and Langmuir D. (1986) Adsorption of Cu, Pb and Zn by δ-MnO_2: applicability
463 of the site binding-surface complexation model. *App. Geochem.* **1,** 255-264.
464 Charlton S.R., and D.L. Parkhurst D.L. (2002) *PhreeqcI—A graphical user interface to the*
465 *geochemical model PHREEQC.* U.S. Geological Survey Fact Sheet FS- 031-02.
466 Coale K.H., and Bruland K.W. (1988) Copper complexation in the northeast Pacific. *Limnol.*
467 *Ocean.,* **33**, 1084-1011.
468 Cronan D.S. (1969) Inter-element associations in some pelagic deposits. *Chem. Geol.*, **5**, 99-
469 106.
470 Dent, A. J., and Mosselmans, J. F. W. (1992) *A guide to EXBACK, EXCALIB, and*
471 *EXCURV92.* Daresbury Laboratory, Warrington, U.K.
472 Drits V.A., Silvester, E., Gorshkov A.I., and Manceau A. (1997) Structure of synthetic

473 monoclinic Na-rich birnessite and hexagonal birnessite: I. Results from X-ray
474 diffraction and selected-area electron diffraction, *Am. Mineral.* **82**, 946–961.
475 Dzombak D. A., and Morel F.M. (1990) *Surface Complexation Modelling: Hydrous ferric*
476 *oxide.* Wiley-Interscience, New York.
477 Fu G.M., Allen H.E., and Cowan C.E. (1991) Adsorption of cadmium and copper by
478 manganese oxide. *Soil Sci*., **152**, 72-81.
479 Grangeon S., Lanson B., Lanson M., and Manceau A. (2008) Crystal structure of Ni sorbed
480 synthetic vernadite: a powder x-ray diffraction study. *Min. Mag.* **72**, 1279-1291.
481 Hedin L., and Lundqvist S. (1969) Effects of electron-electron and electron-phonon
482 interactions on the one-electron states of solids. *Solid State Phys.* **23**, 1-181.
483 Hiemstra T., and Van Riemsdijk W.H. (1996). A surface structural approach to ion
484 adsorption: the charge distribution (CD) model. *J. Colloid Interface Sci.* **179**, 488–
485 508.
486 Jones L.H.P., and Milne A.A. (1956) Birnessite, a new manganese oxide mineral from
487 Aberdeenshire, Scotland. *Mineral. Mag.* **31**, 283-288.
488 Kumar R., Das S.K., Ray R.K., and Biswas A.K. (1994) A SEM backscattered electron
489 mode study of microstructural features of ferromanganese nodules from central indian
490 ocean basin. *Trans. Indian Institute of Metals* **47**, 273-285.
491 Lanson B., Drits V.A., Silvester E., and Manceau A. (2000) Structure of H-exchanged
492 hexagonal birnessite and its mechanism of formation from Na-rich monoclinic
493 buserite at low pH, *Am. Mineral.* **85,** 826–838.
494 Lanson B., Drits V.A., Gaillot A.C., Silvester E., Plancon A., and Manceau A. (2002)
495 Structure of heavy-metal sorbed birnessite: Part I. Results from X-ray diffraction. *Am.*
496 *Min.* **87**, 1631-1645.
497 Manceau A., Lanson B., and Drits V. A. (2002) Structure of heavy metal sorbed
498 birnessite. Part III: Results from powder and polarized extended X-ray absorption fine
499 structure spectroscopy. *Geochim. Cosmochim. Acta* **66**, 2639-2663.
500 Manceau A., Lanson M., and Geoffroy N. (2007) Natural speciation of Ni, Zn, Ba, and As in
501 ferromanganese coatings on quartz using X-ray fluorescence, absorption, and
502 diffraction. *Geochim. Cosmochim. Acta* **71**, 95-128.
503 McKenzie, R.M. (1989) Manganese oxides and hydroxides. In: Dixon J. B. and Weed S. B.
504 (Eds.). Minerals in soil environments. Soil Science Society of America, Madison,
505 Wisconsin. pp. 493-502.

506 Morel F., and Morgan J. (1972) Numerical method for computing equilibria in aqueous
507 chemical systems. *Environ. Sci. Technol.* **6**, 58-67.
508 Moffett J.W., and Dupont C. (2007) Cu complexation by organic ligands in the sub- arctic
509 NW Pacific and Bering Sea. *Deep Sea Res. Part I,* **54,** 586-595.
510 Murray J.W., Balistrieri L.S., and Paul B. (1984) The oxidation state of manganese in marine
511 sediments and ferromanganese nodules, *Geochim. Cosmochim. Acta* **48**. 1237–1247.
512 Parkhurst D.L., and Appelo,C.A.J. (1999) *User's guide to PHREEQC (version 2)--A computer*
513 *program for speciation, batch-reaction, one-dimensional transport, and inverse*
514 *geochemical calculations: U.S. Geological Survey Water-Resources Investigations*
515 *Report 99-4259*, 312 p.
516 Pasquarello A., Petri I., Salmon P.S., Parisel O., Car R., Toth E., Powell D.H., Fischer H.E.,
517 Helm L., and Merbach A.E. (2001) First solvation shell of the Cu(II) aqua ion:
518 evidence for fivefold coordination. *Science* **291**, 856–9.
519 Peacock C.L. (2009) Physiochemical controls on the crystal chemistry of Ni in birnessite:
520 genetic implications for ferromanganese precipitates. *Geochim. Cosmochim. Acta*,
521 **73**, 3568-3578.
522 Peacock C.L., and Sherman D.M. (2007a) Sorption of Ni by birnessite: equilibrium controls
523 of Ni in seawater. *Chem. Geol.*, **238.** 94-106
524 Peacock C.L., and Sherman D.M. (2007b) Crystal chemistry of Ni in marine ferromanganese
525 crusts and nodules. *Am. Mineral.* **92**,1087-1092.
526 Perdew J.P., Chevary J.A., Vosko S.H., Jackson K.A., Pederson M.R., Singh D.J.,
527 and Fiolhais C. (1992) Atoms, molecules, solids, and surfaces – applications of the
528 generalised gradient approximation for exchange and correlation. *Phys. Rev. B* **46**,
529 6671-6687.
530 Perdew J.P., Burke K., and Ernzerhof M. (1996) Generalized gradient approximation made
531 simple. *Phys. Rev. Lett.* **77**, 3865-3868.
532 Post, J.E., 1992. Crystal structures of manganese oxide minerals. In: Skinner H. C. W. and
533 Fitzpatrick R. W. (Eds.). Biomineralization Processes: Iron, Manganese. Catena
534 Supplement 21, Catena, Cremlingen-Destedt, Germany. pp. 51-73.
535 Sherman D.M., Peacock C.L., and Hubbard C.G. (2008) Surface complexation of U(VI) on
536 goethite (-FeOOH). *Geochim. Cosmochim. Acta* **72**, 298-310.
537 Sherman D.M. (2009) Surface complexation modelling: mineral-fluid equilibria at the

538 molecular scale. *Rev. Mineral Geochem.*, **70**, 181-205.
539 Silvester E., Manceau A., and Drits V.A. (1997) Structure of synthetic monoclinic Na-rich
540 birnessite and hexagonal birnessite: II. Results from chemical studies and EXAFS
541 spectroscopy, *Am. Mineral.* **82**, 962–978.
542 Stern E. A. (1993) Number of relevant independent points in X-ray absorption fine-structure
543 spectra. *Phys. Rev. B* **48**, 9825-9827.
544 te Velde, G., Bickelhaupt F.M., Baerends E.J., Fonseca Guerra C., van Gisbergen S.J. A.,
545 Snijders J.G., and Ziegler T. (2001) Chemistry with ADF. *J. Computational. Chem.*
546 **22**, 931-967.
547 Tadanier C.J., and Eick M.J. (2002) Formulating the charge-distribution multisite surface
548 complexation model with FITEQL. Soil Sci Soc Am J 66:1505-1517.
549
550 Villalobos M., Toner B., Bargar J., and Sposito G. (2003) Characterization of the manganese
551 oxide produced by *Pseudomonas putida* strain MnB1. *Geochim. Cosmochim. Acta*
552 **67,** 2649-2662.
553 Villalobos M., Lanson B., Manceau A., Toner B., and Sposito G. (2006) Structural model for
554 the biogenic Mn oxide produced by *Pseudomonas putida*. *Am. Mineral.* **91**, 489–502.
555 Westall J., and Hohl H. (1980) A comparision of electrostatic models for the oxide/solution
556 interface, Adv. Colloid Interface Sci. **12**, 265–294.
557 Van Lenthe E., and Baerends E.J. (2003) Optimized Slater-type basis sets for the elements 1-
558 118. *J. Computational Chem.*, **24**, 1142-1156.
559

560 **Figure Captions**

561

562 FIGURE 1: Sorption of Cu to birnessite (δ-MnO_2) as a function of surface loading (1 wt. %,
563 2.5 wt. % and 5 wt. % Cu maximum adsorbed) and pH. Solid lines are fits from the surface
564 complexation model obtained in this work. Also shown (hollow symbols) are results from
565 previous experiments (Catts and Langmuir, 1986; Fu et al., 1992).

566

567 FIGURE 2: EXAFS spectra (a) and their Fourier transforms (b) of Cu on birnessite at pH 4
568 and pH 8. Spectra were modeled using the clusters shown in Figure 3 with the parameters
569 given in Table 1. Note that the Fourier transforms calculated using EXCURV98 (Binsted,
570 1998) are corrected by Cu-O scattering phase shifts to give approximate actual distances.

571

572 FIGURE 3: Clusters used to model the EXAFS of Cu on birnessite a) cluster with pseudo-C_{3v}
573 symmetry to model Cu as a surface complex over the vacancy b) cluster with pseudo-C_{2v}
574 symmetry to model Cu occupying a vacancy site. The distances were obtained by fitting to
575 the EXAFS spectra.

576

577 FIGURE 4: Optimized geometry of Cu surface complex over a vacancy site on birnessite
578 calculated using density functional theory a) view down z-axis b) view down x-axis c) close-
579 up viewed down the, z-axis showing Cu-O and Cu-Mn distances. Note that oxygens
580 surrounding the vacancy site are protonated unless bonded to Cu.

581

582 FIGURE 5: Optimized geometry of cluster corresponding to Cu occupying a vacancy site.
583 This is the minimum energy structure if all of the the oxygens surrounding the vacancy are
584 deprotonated .

585

Table 1: Cu coordination environment from fits to Cu K-edge EXAFS spectra.

Cluster 1: Surface Complex at pH 4 and 8

	1 **O**	3 **O**	3 **Mn****	3 **Mn****
R	1.95	1.95	3.39	3.43
φ	*0*	*120*	*141*	*123*
θ	*0*	*0, ± 120*	*± 90*	*±30*
$2\sigma^2$	0.024	0.011	0.02	0.02

Cluster 2: Occupied vacancy complex at pH 8

	3 **O**	3 **O**	2 **Mn****	2 **Mn****	2 **Mn****
R	1.87	1.96	2.81	2.94	2.91
φ	*120*	*60*	*90*	*90*	*90*
θ	*0, ± 120*	*180, ± 60*	*± 90*	*±30*	*±150*
$2\sigma^2$	0.019	0.019	0.012	0.012	0.012

*Values in italics are constrained. φ and θ are the spherical coordinates defined as the angles from the z and x axes in Figure 3. **Note that, with the k-range used, distance differences < 0.15 Å between shells are not statistically significant.

Table 2: Surface complexation modelling parameters

Surface area (m^2/g)[a]	107
C_{stern} (F/m^2)[b]	1.0
[$Mn_2O^{-2/3}$] (mol/g)[c]	3.30×10^{-3}
Mineral surface reaction	Equilibrium constant log K
$>Mn_2O^{-2/3} + H^+ = >Mn_2OH^{+1/3}$	2.3[d]
$3>Mn_2O^{-2/3} + Cu^{+2} = (>Mn_2O)_3Cu^0$	5.6[c]
Solution Speciation	
$Cu^{+2} + H_2O = CuOH^+ + H^+$	-7.497[e]
$Cu^{+2} + 2H_2O = Cu(OH)_2 + 2H^+$	-16.196[e]
$2Cu^{+2} + 2H_2O = Cu_2(OH)_2^{+2} + 2H^+$	-10.594[e]

[a]Determined from BET analysis (this study). [b]Fixed (this study). [c]Determined from fitting Cu sorption data (this study) [d]Determined from potentiometric titration (this study). [e] From MINTEQ.V4 database (Charlton and Parkhurst, 2002).

Sherman and Peacock. Figure 1

(one column wide)

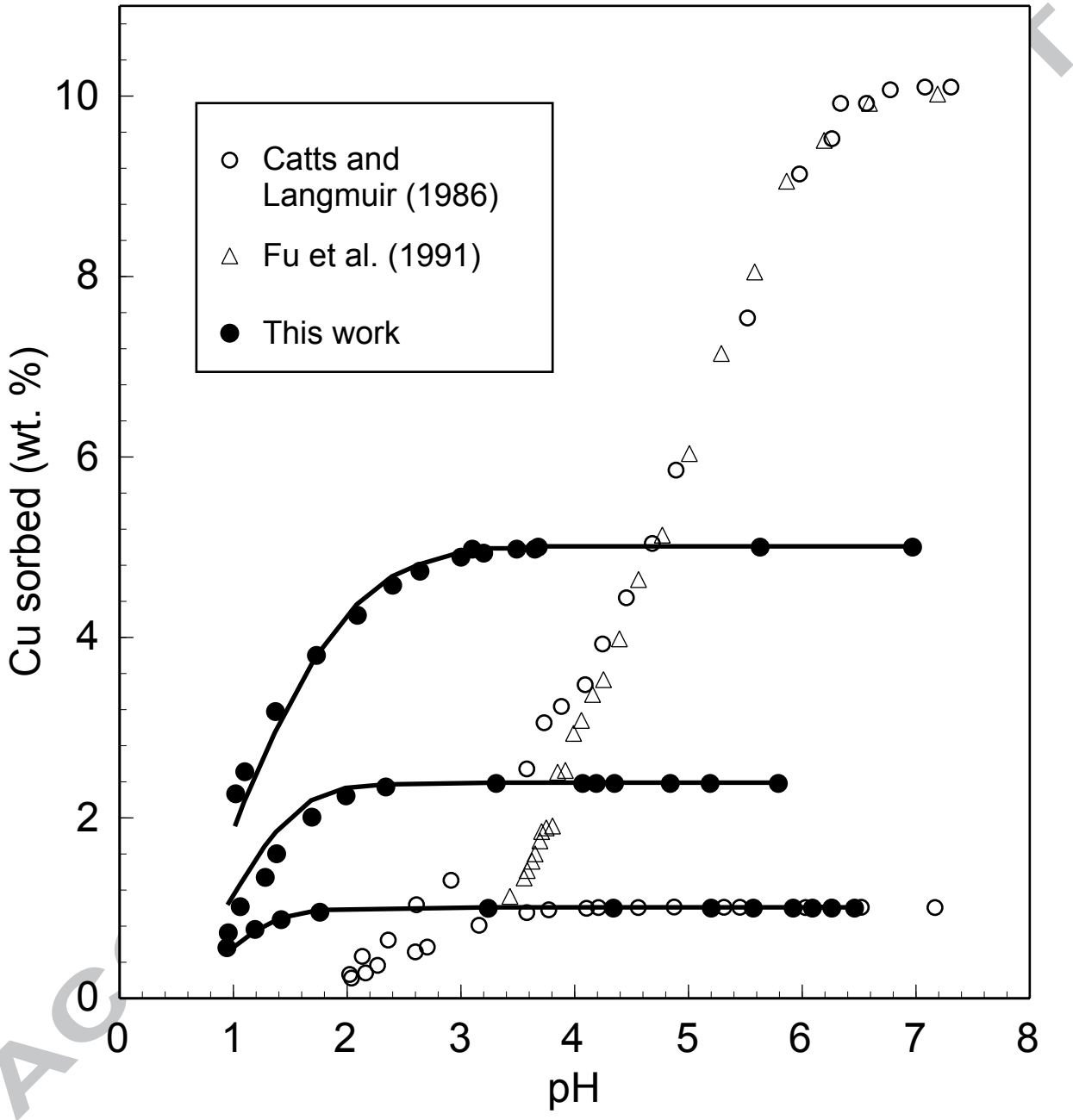

Sherman et al. Figure 2a
(one column wide)

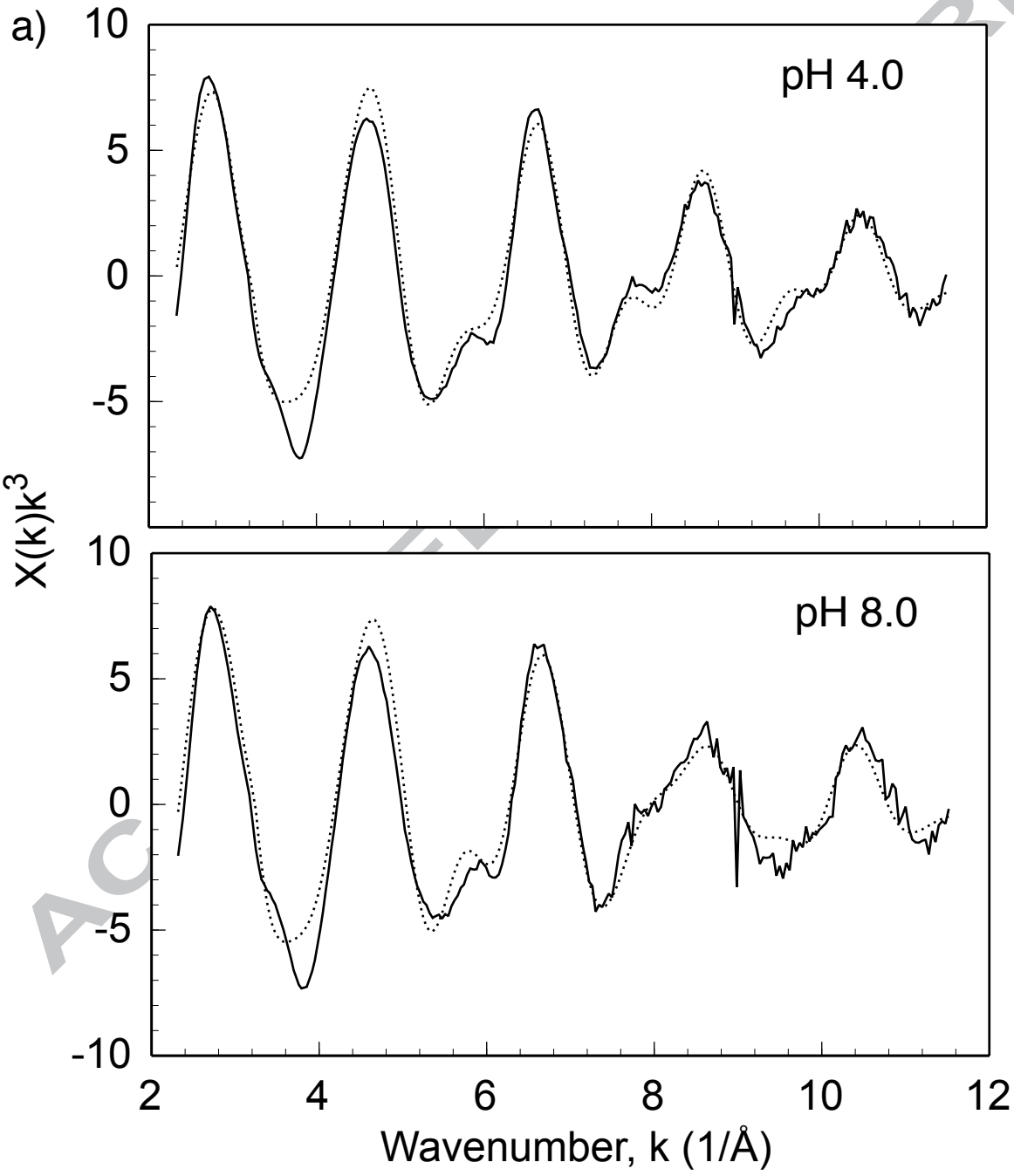

Sherman et al. Figure 2b
(one colume wide)

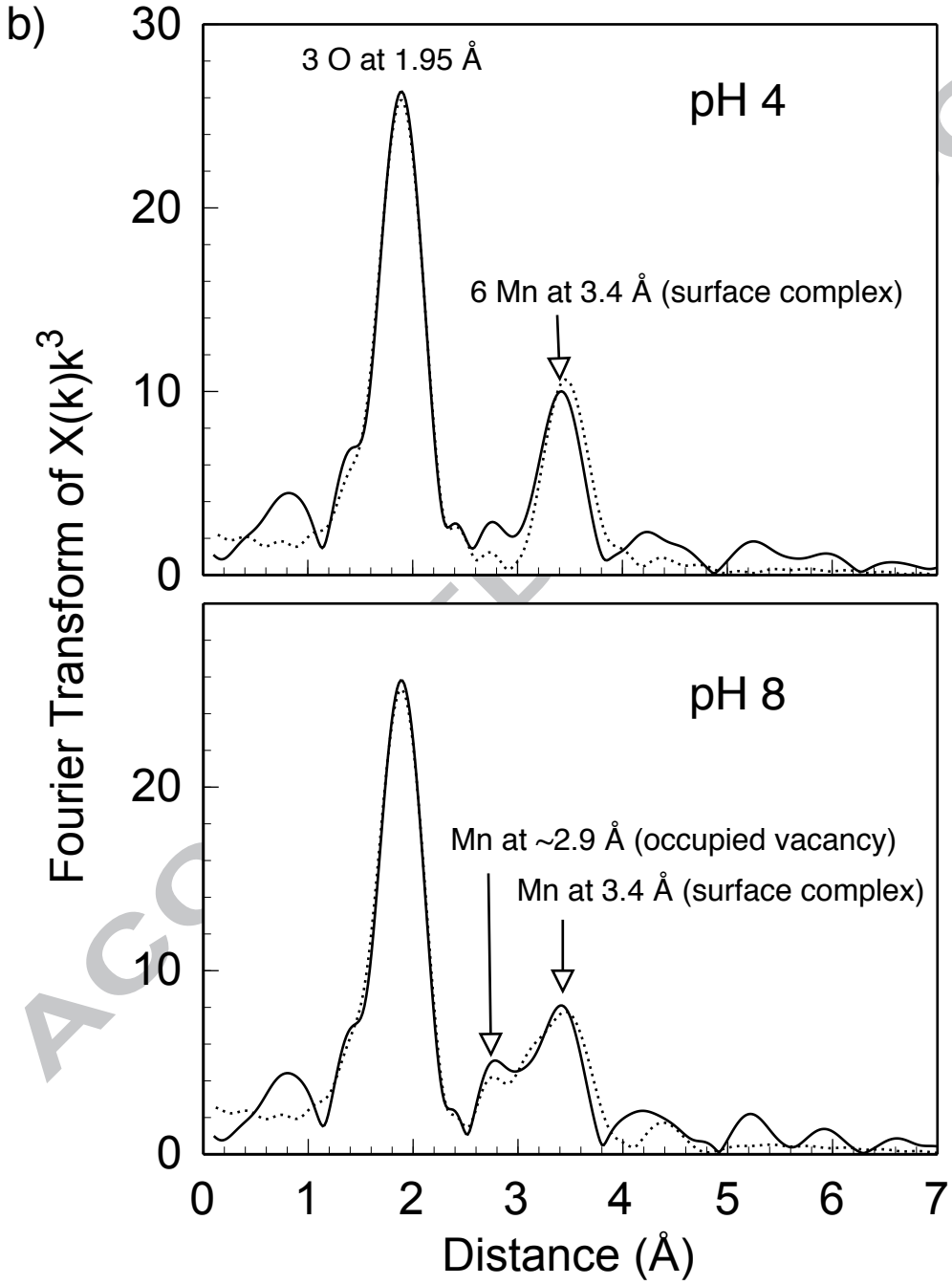

Sherman and Peacock Figure 3 (one column wide)

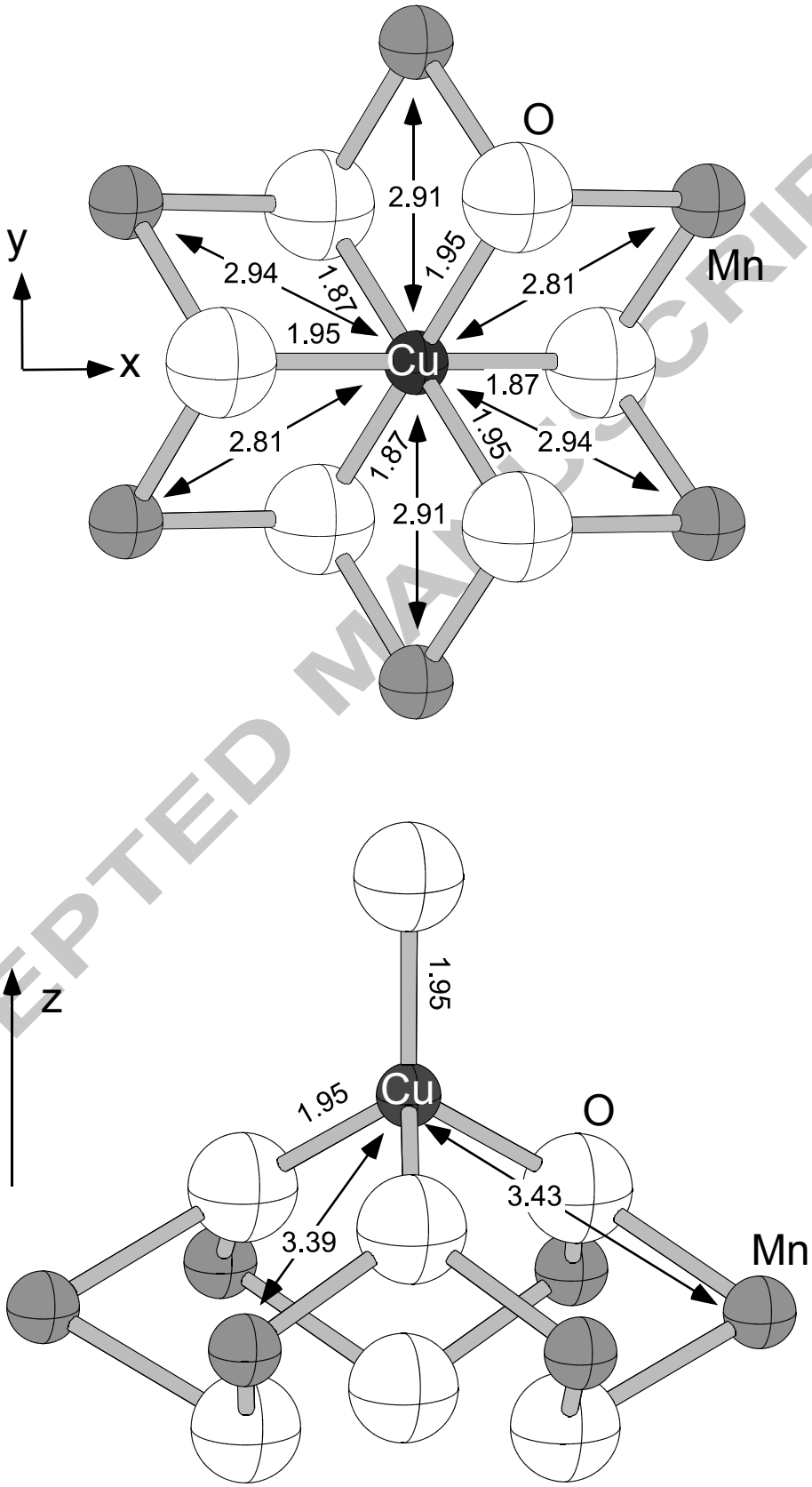

Sherman Figure 4
(one column wide)

a)

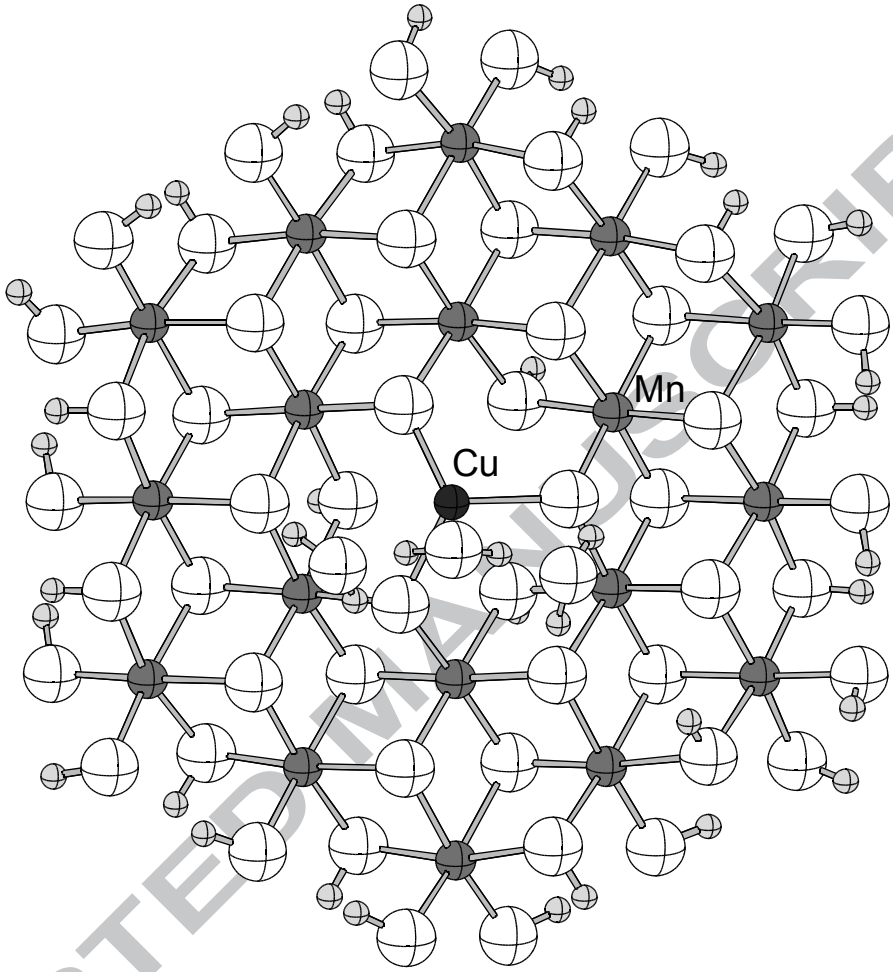

b)

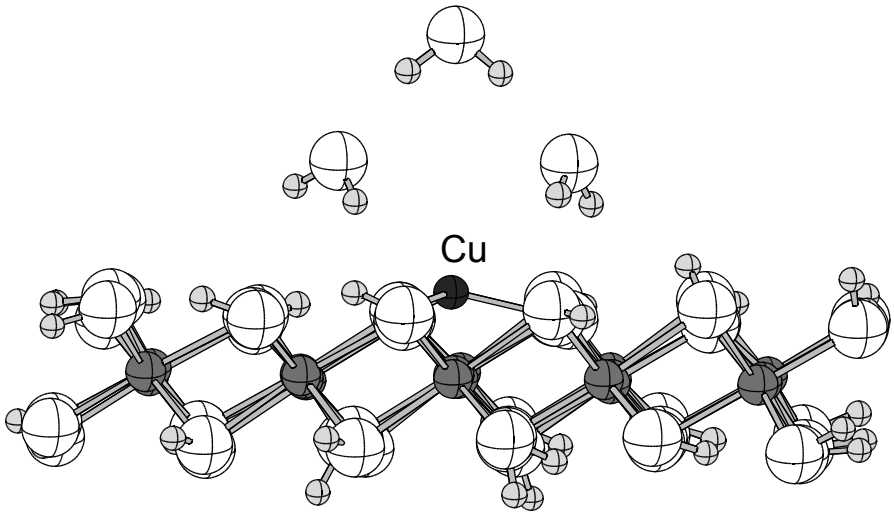

Figure 4c

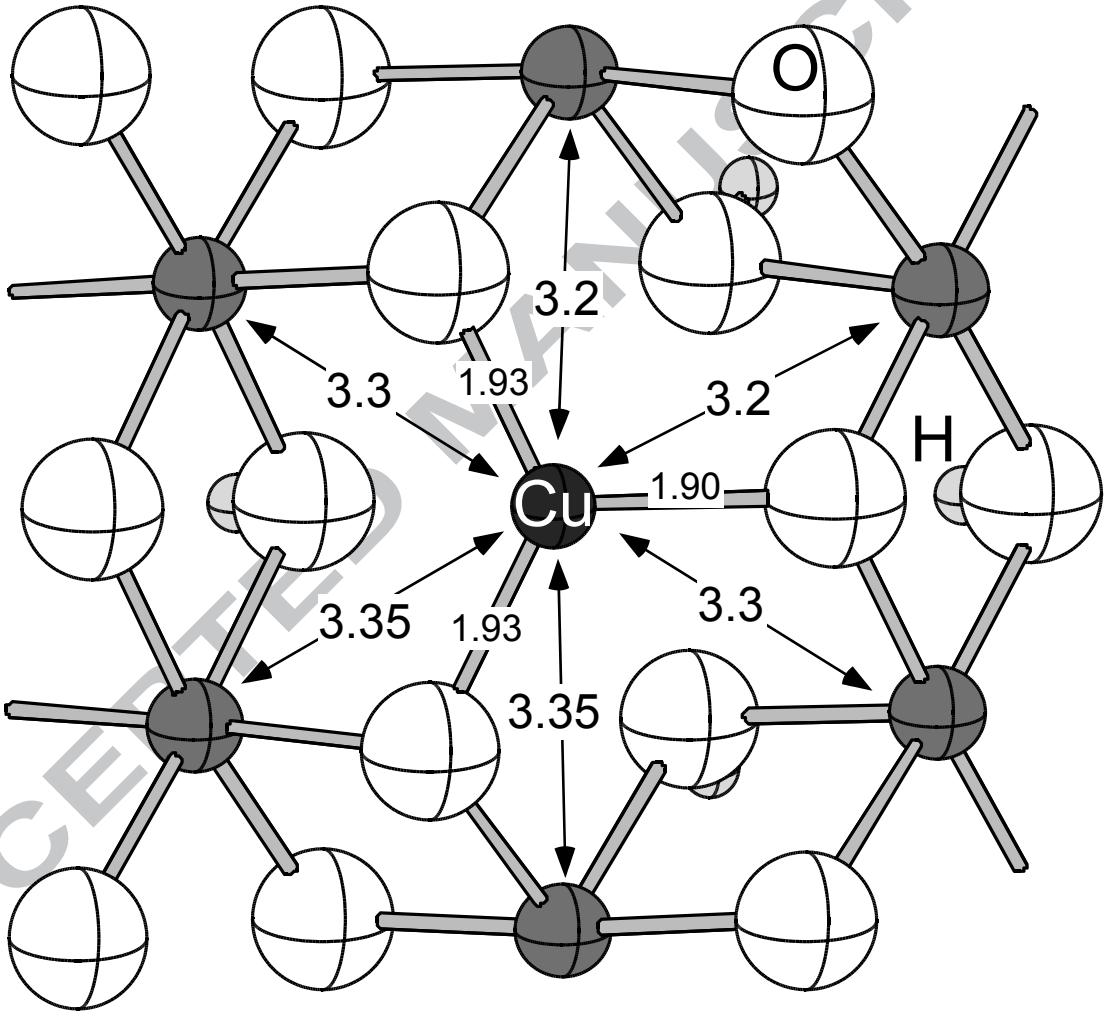

Sherman and Peacock. Figure 5
(one column wide)

a)

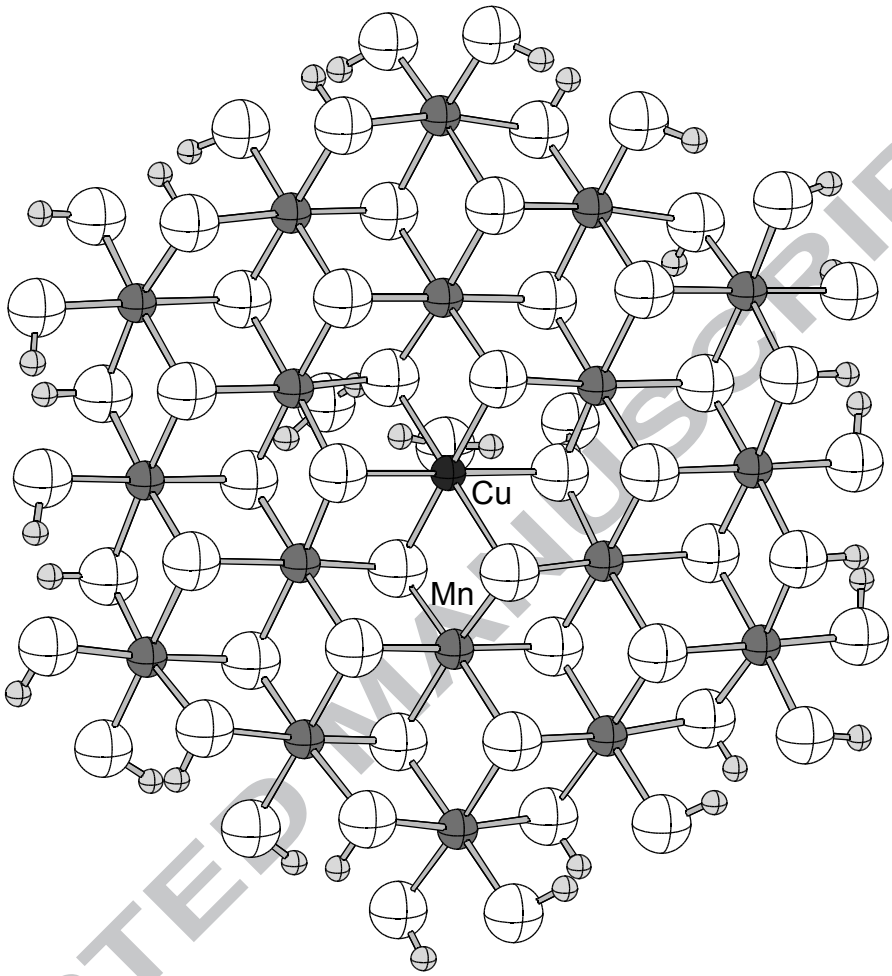

b)